Quantifying microplastic dispersion due to density effects

Ben Stride, Soroush Abolfathi, Gary D. Bending, Jonathan Pearson

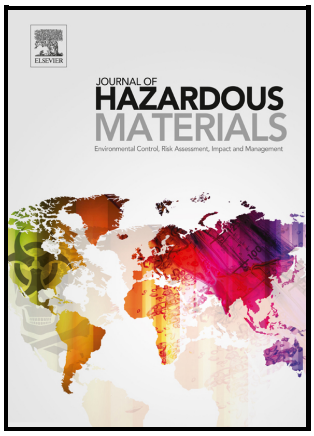

PII: S0304-3894(24)00018-9

DOI: https://doi.org/10.1016/j.jhazmat.2024.133440

Reference: HAZMAT133440

To appear in: *Journal of Hazardous Materials*

Received date: 25 August 2023
Revised date: 20 December 2023
Accepted date: 2 January 2024

Please cite this article as: Ben Stride, Soroush Abolfathi, Gary D. Bending and Jonathan Pearson, Quantifying microplastic dispersion due to density effects, *Journal of Hazardous Materials,* (2024) doi:https://doi.org/10.1016/j.jhazmat.2024.133440

Quantifying microplastic dispersion due to density effects

Ben Stride[a,*], Soroush Abolfathi[a], Gary D. Bending[b], Jonathan Pearson[a]

[a] School of Engineering, University of Warwick, Coventry CV4 7AL, UK

[b] School of Life Sciences, University of Warwick, Coventry CV4 7AL, UK

*Corresponding Author: Ben Stride, E-mail: ben.stride@warwick.ac.uk

Abstract

An experimental study was conducted on how polymer density affects the transport and fate of microplastics in aquatic flows. For the first time, polypropylene (PP), polyethylene (PE), polymethyl methacrylate (PMMA), polyetheretherketone (PEEK), and polyvinyl chloride (PVC) were chemically stained and tested using solute transport techniques and velocities found among rivers in the natural environment (0.016 – 0.361 m/s). The movement of 3D-polymers with densities ranging from 0.9 – 1.4 g/cm^3 was quantified in a laboratory flume scaled to simulate open-channel flows in fluvial systems. Except for PP, in most conditions microplastics exhibited similar transport characteristics to solutes regardless of density and established solute transport models were successfully implemented to predict their transport and fate. Mass recoveries and ADE routing model demonstrated microplastic deposition and resuspension was associated with polymer density below critical velocity thresholds ≤ 0.1 m/s. When density becomes the dominant force at these slower velocities, concentrations of denser than water microplastics will be momentarily or permanently deposited in channel beds and microplastics follow the classical Shields sediment transport methodology. This data is the first to provide microplastic suspension and deposition thresholds based on river velocity and polymer density, making a key contribution to research predicting microplastic fate and organismal exposure.

Keywords

polymer, mixing, emerging contaminant, fluvial hydraulics, sediment transport

Environmental Implications

Microplastics are emerging contaminants that are ubiquitous to aquatic systems. Given their size, microplastics have increased bioavailability and all aquatic organisms can be exposed through direct ingestion, indirect ingestion via prey items, or respiration. Microplastics can act as a pathway for disease-carrying pathogens and many questions remain as to their toxicity. Microplastic transport and fate in fluvial systems is unknown and thereby which organisms experience the most direct exposure. This study aims to reduce the knowledge gap currently associated with how particle properties affect the transport of microplastics in aquatic flows, to ultimately help remediate their impact on the environment.

1. Introduction

Microplastics, plastics > 1 μm and < 5 mm (Frias & Nash, 2019), are now widely recognized as global contaminants in aquatic systems due to several factors including but not limited to their abundance, degradation resistance, ingestible size, pathogen adherence, chemical leaching, and unknown toxicity to humans and the environment (Chamas et al., 2020; Do et al., 2022; Kim & An, 2016; Rehse et al., 2016; Sana et al., 2020; Talbot & Chang, 2022; Yuan et al., 2022; Stride et al., 2023b). All aquatic organisms can be exposed to microplastics through direct ingestion, indirect ingestion via prey items, or by means of respiration (Miller et al., 2020). Microplastics are often collated into one broad “compound” but in fact contain a complex variety of differing physical characteristics such as composition, type, size, shape, and density (Kooi et al., 2018; Onink et al., 2022; Waldschläger & Schüttrumpf, 2019). Whilst moving through aquatic systems microplastics can aggregate and flocculate with each other (de Haan et al., 2019; Wang et al., 2021), enable biofilms to form on their surfaces (He et al., 2022; Hoellein et al., 2019), and

fragment into smaller pieces (Barnes et al., 2009; Pramanik et al., 2021) due to being exposed to many physical, biological, and chemical factors. Accounting for these variables can be challenging when trying to quantify their transport processes (Kooi et al., 2018; Onink et al., 2022; Waldschläger et al., 2022) and ultimately determine their impact on humans and the environment.

Arguably, the most important physical properties that determine microplastic retention within fluvial systems are particle shape, size, biofilm formation, and density (Eerkes- Medrano et al., 2015; Hoellein et al., 2017; Kumar et al., 2021) along with the hydrodynamics of the surrounding water (i.e., laminar or turbulent flow; Kumar et al., 2021) and sediment composition (i.e., clays or gravels; Nizzetto et al., 2016). The impact polymer density has on the fate of microplastics in relation to the other physical properties is unclear. Nizzetto et al's. (2016) theoretical study suggested that microplastics with a diameter of < 200 µm were not retained in the river catchment studied regardless of density and only 16-38 % of microplastics with a higher density than water were retained depending on catchment and soil characteristics. This contrasts with Besseling et al.'s (2017) study which demonstrated for the size class of 1 – 200 µm microplastic retention was strongly associated with polymer density and that particles < 1 µm were not retained. Similarly, Hoellein et al. (2019) found that within different size classes differences in particle density generated a significant variation in settling velocities. Most other microplastic density studies investigated marine systems (Ballent et al., 2013; Coyle et al., 2020; Onink et al., 2022; Suaria & Aliani, 2014) with a higher water density of 1.02 – 1.03 g/cm^3 than freshwater systems (Ziccardi et al., 2016) making comparisons difficult. The dominant impact biofouling has on microplastic fate in aquatic systems is the density change (He et al., 2022) which can be through the increase in mass from the biofilms and attached suspended minerals themselves or the resulting increase in hydrophilicity (Lobelle & Cunliffe, 2011). Both increases and decreases in polymer density have been documented suggesting that the impacts of biofilms on microplastic density are highly influenced by the chemical composition of each polymer (Chen et al., 2019;

Nguyen et al., 2020). No studies have quantified polymer density effects on transport in a controlled environment (to reduce the effects of other aforementioned factors) scaled to simulate real-life fluvial systems such as laboratory flumes. For further information on the literature see text S1.

Microplastics generally have lower particle densities of 0.88 – 1.4 g/cm^3 than natural sediments of 1.5 – 3 g/cm^3 and their density is typically defined through polymer type (Waldschläger et al. 2022). The most produced microplastic polymers are the four types of polyethylene (high-density, medium-density PE, low-density, and linear low-density), polypropylene (PP), polystyrene (PS), and polyvinyl chloride (PVC) which accumulatively account for 65.7 % of the plastic demand in Europe (Plastics Europe, 2022). When including the next most demanded polymers in Europe (polyurethane & polyethylene terephthalate) at least 81.8 % of polymers (excluding thermosets or thermoplastics) contain densities between 0.88 – 1.4 g/cm^3 (Table 1). Given that most microplastics have a density closer to that of water (1 g/cm^3) than natural sediments (1.5 – 3 g/cm^3), plus Chen et al. (2019) and Nguyen et al. (2020) demonstrating relatively minor changes in polymer density through biofilms, solute transport techniques which quantify microplastic density effects based on polymer type may be invaluable to determining microplastic transport and fate in aquatic systems.

The majority of research into the fate of microplastics in fluvial systems has utilized natural sediment theory and thus particle transport models (He et al., 2021; Hoellein et al., 2019; Kooi et al., 2018; Nizzetto et al., 2016; Whitehead et al., 2021) with a smaller number of studies using solute transport theory and focusing primarily on particles of a near neutral buoyancy (Abolfathi et al. 2020; Boos et al., 2021; Cook et al. 2020; Stride et al., 2023). The strength of particle transport models lies in incorporating specific aspects of the particle itself, which is missing from solute transport models. Solute transport models require a well-mixed plume over depth to be valid, which may not be the case for discrete polymers containing different zeta potentials or

densities lighter or heavier than water. Meanwhile, particle transport models do not account for changes as microplastic particles move through a given flow regime and can only observe the behaviour of discrete microplastics in real-time rather than continuous microplastic quantities in real-time like solute transport models. The boundaries of where particle or solute transport models are more applicable to predict microplastic movement need to be investigated in more detail. Shape, size, and density effects on microplastic movement have previously been analysed through settling velocities and deposition rates commonly used for natural particles in both labs and streams (Ballent et al., 2013; Hoellein et al., 2019; Khatmullina & Isachenko, 2017; Mendrik et al., 2023; Waldschläger & Schüttrumpf, 2019; Wang et al., 2021). Settling velocity can help identify deposition rates of microplastics in both field studies and numerical simulations (Khatmullina & Isachenko, 2017, Waldschläger & Schüttrumpf, 2019), but settling velocity only analyses the speed a particle reaches as it falls through a fluid and not the variances of a particles characteristics or their distribution as they travel through a given flow regime.

This study investigates the effects of particle density on the transport dynamics of microplastics in open channels. This is with the aim of quantifying specific microplastic fate thresholds based on density and velocity while addressing the knowledge gap currently associated with how polymer density affects the transport and fate of microplastics in aquatic flows. Cook et al's. (2020) microplastic staining technique using Nile red dye was adopted to trace five polymers with densities ranging from 0.9 g/cm^3 to 1.4 g/cm^3 within the 20 - 200 µm micro-size class defined by Bermúdez & Swarzenski (2021). Fluorometric techniques were employed using Rhodamine WT fluorometers equally spaced over depth at each station, to determine concentration differences over depth, and discover where the assumption of a well-mixed plume is valid in a laboratory flume designed to simulate open-channel flow (Fig.1). Well-established solute transport models based on the advection-dispersion equation (ADE) were implemented to quantify both solute and microplastic mass recovery (MR), shear dispersion, and longitudinal

dispersion coefficients (D_x). Velocities collected through an Acoustic Doppler Velocimeter (ADV) were used to theoretically predict D_x. The data and techniques can then be used to inform future water quality projects of the fate of microplastic polymers in freshwater environments.

2. Methods

2.1 Experimental Setup

Experiments were conducted in a 0.30 m wide, 15 m long recirculating tilting Armfield flume with a depth ranging from 0.25-0.254 m due to the variability at higher discharges (Fig. 1). The total flume length was 18.05 m long and contained a series of rotating shafts that could be used to adjust the bed slope. A consistent bed slope of 0.0020 (1/500) was used across the different experimental velocities. The downstream sluice gate was altered to maintain a flow depth of 0.25-0.254 m at different discharges by turning the handle above. A honeycomb structure was implemented to straighten the flow and prevent any phenomena influencing the velocity profile (Stride et al., 2023a). The injection point was located at the flow inlet to ensure the tracer cloud was fully mixed before entering the main flow length. 10 ml of Rhodamine WT at 10000 ppb or 2 g of Nile red stained microplastics with < 20 ml of water was well-mixed into a syringe before each injection. Separate syringes were used for each polymer and the flume and storage tanks were emptied, cleaned, and refilled between discharge adjustments to prevent cross-contamination of test runs, which were performed individually for each polymer and Rhodamine WT dye. Fig. 1 shows a 2D plan view of the length side of the flume with the flow direction going from left to right.

The ADV was positioned near the center of the flow length section to record 3D water velocity measurements over depth (Fig. 1). A high-power level at 100 Hz for a 30-second duration and a range to last cell of 72 mm was implemented, including a cell range of 32 mm consisting of eight cells with a thickness of 4 mm. Data with averaged SNR values < 30 and correlation values < 80 across all four beams were considered susceptible to pulse interference and removed.

Spikes in the ADV data were highlighted using a threshold calculated from the surrounding datapoints and interpolated (along with low SNR and correlation values) using the mean of the surrounding data points or the total mean if adjacent to each other in line with methods employed by Goring & Nikora (2002). Velocity profiles were calculated by fitting a logarithmic curve through the measured data points and theoretically predicted using logarithmic law by rearranging Eq. (1):

$$u_* = \frac{uk}{LN\left(\frac{H}{y_0}\right)}, \quad (1)$$

where u_* represents shear velocity from the bottom of the channel (m/s), u is the velocity (m/s), k is the Von Karman constant, H is the mean channel depth (m), and y_0 is the relative roughness of the channel bed (depending on the material) divided by 30 for hydraulically rough flows.

Discharges (Q) were set via a SIEMENS F M MAG6000 electromagnetic flow meter adjusted by turning the worm and wheel gate valve located in the pipe between the pump and flow meter. Four replicates (n) at seven discharges ranging from 0.001 – 0.027 m³/s were implemented in accordance with Cook et al. (2020), enabling a direct comparison, with the addition of a slower Q of 0.001 m³/s to closer examine polymer density effects at slower velocities (Table 2). Concentration data was gathered at time intervals every 0.5 seconds (2 Hz) for 0.001 m³/s, 0.2 seconds (5 Hz) for 0.002 m³/s, and 0.1 seconds (10 Hz) for discharges of 0.007 m³/s and above through an automatic recorder logging voltage changes in the water column. Turner Designs Cyclops-7 fluorometers were positioned at 3.0 m intervals, with a 9.0 m distance from the first to fourth station, and at 90º angles ensuring maximum detection of the tracer cloud within a specific depth within the water column. As illustrated by grey rectangles emitting green light in the experimental setup above, twelve fluorometers were used in total and split over four stations (Fig. 1). Three fluorometers were positioned at each station, one at the bottom of the water column, one in the middle, and one at the top allowing three dispersion coefficients to be calculated for each temporal concentration distribution. This was implemented with the aim of

analysing possible dispersion differences, due to the different microplastic densities potentially producing different concentrations over depth.

2.2 Microplastics

Five 3D-spherical polymers with different densities ranging from 0.9 – 1.4 g/cm³ were stained with Nile red dye and calibrated for each fluorometer (Fig. S1): PP (TEC03CON346, Goonvean Fibres) of 90 µm in diameter and 0.9 – 0.91 g/cm³ density, PE (434272, Sigma-Aldrich) of 40 – 46 µm in diameter and 0.94 g/cm³ density, polymethyl methacrylate (PMMA; 463183, Sigma-Aldrich) of 50 µm in diameter and 1.19 g/cm³ density, polyetheretherketone (PEEK; 430-005-24, Goodfellow) of 80 µm in diameter and 1.26 – 1.32 g/cm³ density, and PVC (81387, Sigma-Aldrich) of 63 – 150 µm in diameter and 1.4 g/cm³ density. The specific microplastic staining process is outlined in Cook et al. (2020). Sieving in line with methodology used for natural sediments (Waldschläger et al., 2022) was utilized to ensure particle sizes agree with the specifications provided by manufacturers. Four sieves with pore sizes of 38 µm, 63 µm, 90 µm, and 150 µm were employed. All polymers except PVC passed through the 90 µm sieve with portions of the others also passing through 63 µm (38 < 90 µm). PE was the only polymer for all its mass to pass through the 63 µm pore size making it the smallest (38 < 63 µm) and most consistent in relation to manufacturer specifications. PVC's diameter was the largest and had the greatest range (63 < 150 µm). Rhodamine WT dye was employed as the representative solute to be used as a comparison to the dispersion of microplastics.

To test the fluorescence of the Nile Red stained microplastics, calibrations were performed using the Turner Designs Cyclops-7 fluorometers (Fig. S1) at a x1 or x10 gain within a 5-litre beaker and a blacked-out background. This tested the quality of the measurements recorded using the fluorometers to minimize any uncertainty in the data collected. Solutions were stirred during each calibration using a Heidolph overhead stirrer to enable microplastic concentrations to be well-mixed over depth regardless of density. Denser microplastics such as PEEK and PVC

were stained a darker shade of pink while lighter microplastics such as PP and PE were stained a lighter shade as a result of the chemical impregnation process (Fig. S2). This phenomenon caused the denser microplastics to produce higher voltages relative to their concentrations, illustrated by the total mean calibration curves for each polymer in Fig. 2 due to them emitting and exciting different wavelengths of light.

As a result, the sensitivity of the Cyclops-7 fluorometers (built for Rhodamine WTs wavelengths) for detecting each polymer varies. Fig. 2 plots concentration against the mean voltage of all twelve Cyclops-7 fluorometers to calculate the mean gradient of each polymer. The higher the gradient the greater the ability for the fluorometers to detect polymer concentrations. This makes PEEK (5.4196x + 0.115) the closest shade of pink to Rhodamine WT dye and the easiest polymer for Rhodamine Cyclops-7 fluorometers to detect. Therefore, lower concentrations of PEEK can be injected relative to the other polymers to be accurately traced. Consequently, the inverse is also true with PP demonstrating a shallow gradient of 0.1805x + 0.003 thus potentially requiring higher initial concentrations when injected.

Velocities for Rhodamine WT dye and each microplastic were calculated relative to the position of each region over depth in the water column through Eq. (2) and highlighted in Fig. 1 as F1 - F4 for the bottom, F5-F8 for the middle, and F9-F12 for the top fluorometers.

$$u = \frac{x_4 - x_1}{\mu_4 - \mu_1}, \quad (2)$$

where x_4 and x_1 represent the distance from the inlet (the location of the fourth and first fluorometers; m) and μ_4 and μ_1 is the travel time between the centroids (s) of the fourth and first fluorometers respectively. Reynolds numbers for each velocity were calculated through Eq. (3) and determine the turbulence exhibited on each concentration:

$$Re = \frac{uH}{v}, \quad (3)$$

where v is the kinematic viscosity (m²/s).

2.3 Data Analysis

With Cyclops-7 fluorometers varying in their sensitivity to each microplastic, despite the flume and storage tanks being constantly cleaned and refilled, spikes did occur in the concentration data for less-sensitive polymers due to the recirculating flume and thus the nature of the experiment. This was because minute amounts of more-sensitive polymers were resuspended during their test runs at higher discharges that resuspended retained microplastics into the main flow length. Concentration spikes in each dataset were identified, removed, and interpolated using a threshold and mean calculated from the surrounding data points. Background removal of concentration data was applied by subtracting the mean of the first 30 seconds of data collection for each concentration curve. Smoothing was implemented through a running average containing 1 % of the total number of data points, enabling a larger or smaller window to be implemented depending on the logging length/discharge. Confidence intervals of all concentration data analyses were determined by calculating the standard deviation (σ^2) and applying an α value of 5%.

D_x was used to describe the change in characteristics of a tracer cloud as it travels in the longitudinal direction by applying Taylor's (1954) original analysis for calculating the longitudinal dispersion of a solute or vertically well-mixed particle within turbulent flow. D_x was generated from the temporal concentration distribution of each tracer injection through Fischer's (1966) equation:

$$D_x = \frac{1}{2} u^2 \frac{d\sigma_t^2}{dt}, \quad (4)$$

where (σ_t^2) is the standard deviation of the response curves and t is time (s). Cutoff values for the start and end of the peaks were selected using approximately 5% of the peak concentration and were checked by plotting the values on the respective distributions. Moments of the distributions were calculated (Rutherford, 1994) and a regression was fitted to calculate the

gradient of time to centroid against the variance where only values with an R^2 > 0.8 were accepted. Where no R^2 values were greater than 0.8, the highest value within that section of the water column was implemented and highlighted for reference.

Through Rutherford's (1994) moments, the MR of a pulse injection was achieved by dividing the first moment of area (M_0) at the last station by M_0 in the first, then multiplying the answer by 100. This was with the aim of calculating how much of the injected dye or microplastic mass exited the system and how much had been retained. For the slow discharges of 0.001 m³/s and 0.002 m³/s, moments and velocities were calculated from the second station instead of the first to ensure full mixing over depth at slower velocities. With u_* being known, a factor ($\frac{D_x}{Hu_*}$) can be estimated as a measure of shear dispersion generated by the channel bed for each microplastic in the longitudinal direction and compared to Elder's (1959) theoretical 5.93 factor for mixing in uniform open channels. To validate observed dispersion coefficients, it is important to compare them to predicted coefficients based off proven theoretical methods that utilize the hydraulic parameters of the system. Elder's (1959) proven equation can theoretically predict D_x by accounting for the effects of shear dispersion in Eq. (5):

$$D_x = 5.93Hu_*, \quad (5)$$

u_* was calculated through dividing the depth-averaged velocity u by between 10 and 20 depending on the roughness of the channel bed, with 10 being rough and 20 being smooth (Rutherford, 1994). However, velocity profiles for Elder's (1959) equation must obey logarithmic law over the vertical as it does not account for fluctuations in velocity like Chikwendu's (1986) *N*-zone model.

Chikwendu's (1986) *N*-zone model divides the channel cross-section into an infinite number of zones (j) and thus considers potential changes in velocity over depth in agreement with Taylor's (1954) original formulas. Mixing in each zone is dependent on the velocity

differences of the zones either side of it $\left(q_1+q_2+\cdots+q_j\right)^2\left[1-\left(q_1+q_2+\cdots+q_j\right)\right]^2\left[u_{1,2\ldots j}-u_{(j+1)\ldots N}\right]^2$ divided by the vertical diffusivity $b_{j(j+1)}$ with the longitudinal diffusivity $\sum_{j=1}^{N} q_j D_{xj}$ added to the total

$$D_x(N)=\sum_{j=1}^{N-1}\frac{\left(q_1+q_2+\cdots+q_j\right)^2\left[1-\left(q_1+q_2+\cdots+q_j\right)\right]^2\left[u_{1,2\ldots j}-u_{(j+1)\ldots N}\right]^2}{b_{j(j+1)}}+\sum_{j=1}^{N} q_j D_{xj}, \quad (6)$$

where $j=(1,2,\ldots N)$, $q=\frac{h_j}{H}$, D_{xj} is the average longitudinal diffusivity, and h_j is the thickness of each zone. The average vertical diffusivity between each zone is calculated by

$$b_{j(j+1)}=\frac{2D_{zj(j+1)}}{H^2\left(q_j+q_{j+1}\right)}, \quad (7)$$

where $D_{zj(j+1)}=Hku_*q(1-q)$ using Elder's (1959) equation for vertical diffusivity or $D_{zj(j+1)}=\frac{ku_*H}{6}$ when using a depth-averaged value (Jobson & Sayre, 1970).

u_* is a representation of shear stress and was used to calculate critical shear stress (u_{*c}) to determine the incipient motion of solid particles such as microplastics. Critical shear stress values were compared to Shields (1936) and Miller et al. (1977) curves in line with sediment transport theory to enable a direct comparison between solute and sediment transport techniques. The Shields (1936) and Miller et al. (1977) curves predict the conditions where sediment starts to move using a dimensionless Shields parameter (θ) and the particle Reynolds number (Re_*):

$$\theta=\frac{\tau}{(\rho_s-\rho)\mathrm{g}D}, \quad (8)$$

$$Re_*=\frac{u_*D}{v}, \quad (9)$$

where τ is the shear stress and can be calculated by $\tau=u_{*c}^2$, ρ_s is the particle density (kg/m³), ρ is the fluid density (kg/m³), g is acceleration due to gravity (m²/s), and D is the particle diameter (m). This method cannot be used for polymers with densities < 1 g/cm³ because it was designed

for sediments with densities greater than water and $(\rho_s - \rho)$ would be negative resulting in negative θ values.

Another common method to predict mixing in fluvial systems are routing procedures that model concentration distributions of observed data. The standard method within open channels is the ADE routing model that quantifies the downstream concentration distribution $c(x_2, t)$ by using the upstream trace $c(x_1, t)$:

$$c(x_2, t) = \int_{\gamma=-\infty}^{\infty} \frac{c(x_1,\gamma)u}{\sqrt{4\pi D_x(\bar{t}_2 - \bar{t}_1)}} exp\left[-\frac{u^2(\bar{t}_2 - \bar{t}_1 - t + \gamma)^2}{4D_x(\bar{t}_2 - \bar{t}_1)}\right] d\gamma, \quad (10)$$

where γ is the integration variable. $\bar{t}_i$ is the travel time between the centroids of the distributions given through Eq. (11) and dt is the distance covered by each concentration:

$$\bar{t}_i = \frac{\int_{t=-\infty}^{\infty} tc(x_i,t)dt}{\int_{t=-\infty}^{\infty} c(x_i,t)dt}. \quad (11)$$

An R_t^2 parameter can then be utilized to quantify the goodness of fit of a predicted downstream temporal concentration profile $p(x_2, t)$ in relation to the measured downstream data $c(x_2, t)$:

$$R_t^2 = 1 - \left[\frac{\sum_{t=1}^{n}[c(x_2,t) - p(x_2,t)]^2}{\sum_{t=1}^{n} c(x_2,t)^2}\right]. \quad (12)$$

An R_t^2 value of 1.0 indicates a perfect fit from the model in question and values less than 1.0 indicate a weaker predictive capability depending on what is classified as an accurate R_t^2 (Guymer & Stovin, 2011).

3. Results

3.1 Response Curves

PP's shallow gradient of 0.1805x + 0.003 (see §2.2) required higher initial concentrations when injected and could not be sufficiently detected when compared to background concentrations for analysis. The microplastic staining method needs to be adapted or

fluorometers with different optics need to be used so PP can be detected within laboratory flumes containing a large volume of water. At faster velocities it was unclear as to whether this was a result of the staining and detection process or the bulk of the concentration mass missing the fluorometers by being suspended at the water surface, or a combination of both. In many cases small PP response curves could be detected at the first station but not the second or third. An image analysis was implemented to provide a qualitative investigation into PP transport (see §3.4). PVC could not be detected for the slowest depth-averaged velocity of 0.016 m/s and by the top and middle fluorometers at 0.031 m/s (Table 2). Example response curves for the depth-averaged velocity of 0.235 m/s (0.017 m³/s) are shown in Fig. 3 with R_t^2 values for all discharges and corresponding depth-averaged velocities displayed in Table 2. The ADE model struggled to predict the mixing of PMMA and PEEK at 0.016 - 0.031 m/s with R_t^2 varying from 0.268 – 0.908 and had zero capability for PVC at 0.016 - 0.101 m/s. All other concentrations had R_t^2 > 0.95 except for PE at 0.361 m/s and PVC at 0.3 m/s. When averaged across all polymers R_t^2 was between 0.959 – 0.968 depending on whether the bottom, middle, or top fluorometers were used. Positioning the fluorometers at different depths over the vertical had no effect on the predictive capability of the ADE. The ADE model had the lowest mean R_t^2 for PVC at 0.939 with the other polymers all between 0.966 – 0.980.

Fig. 4 illustrates the first attempt to quantify microplastic recovery percentages through a range of velocities experienced in rivers worldwide. MR was lowest for PVC at slower velocities of 0.016 - 0.101 m/s and for PMMA and PEEK for the slowest velocities of 0.016 - 0.031 m/s (Fig. 4). Approximately 100 % of PVC mass was retained within the main flow section for 0.016 m/s and at 0.031 m/s for the top and middle fluorometers, where only 7.95 ± 22.86 % reached the bottom fluorometer at the fourth station (hence the large CI) when averaged. PMMA and PEEK displayed similar recover percentages throughout where 72.92 ± 20.63 – 87.41 ± 13.55 % reached the fourth station for 0.016 - 0.031 m/s and at least 93.71 + 9.51 for all other velocities. PMMA

and PEEK's MR at 0.016 - 0.031 m/s decreased from ≥ 100 % at the water surface to between 43.08 - 49.33 % for 0.016 m/s and 67.18 – 81.52 % for 0.031 m/s at the channel bed, with this difference being highlighted in Fig. S3. PE exhibited similar MR to Rhodamine WT dye and both exhibited no differences with velocity (Fig. 4).

Where PMMA, PEEK, and PVC had reduced MR for slower depth-averaged velocities, the MR for the bottom fluorometers was most affected with no changes in top fluorometer MR for PMMA and PEEK (Fig. S4). MR showed the greatest variability for PVC and was near to 100 % for all polymers at velocities of 0.169 m/s or greater (Fig. 4). Two-Factor ANOVA's with replication revealed a significant difference in MRs between polymers across all velocities (p-value < 0.05) and no significant difference was found across all velocities when PVC was removed (p-value > 0.05). No significant difference was found for velocities ≥ 0.101 m/s (including PVC) although a significant difference was found for MR over depth between the bottom, middle, and top fluorometers (p-value < 0.05). No significant MR differences were found over depth or between polymers for velocities ≥ 0.169 m/s (p-value > 0.05).

3.2 Hydraulic Characteristics

Depth-averaged velocities and corresponding Reynolds numbers for each discharge are presented in Table 2. Measured, fitted, and theoretical mean velocities for each ADV setup for all discharges are shown in Fig. 5, with all velocities for each ADV setup shown in Fig. S5. Distinct bands can be seen for each ADV setup in Fig. S5 due to the nature of the equipment which made little difference to the resulting fitted velocity profiles when averaged in Fig. 5. Velocity differences over depth increased with discharge for 0.007 m^3/s and above, with faster velocities closer to the water surface and slower velocities near the channel bed. Velocity profiles for 0.001 m^3/s and 0.002 m^3/s exhibited very little change over depth with the difference between the bottom and top measurements by the ADV being just 0.00072 m/s and 0.00213 m/s for each discharge respectively compared to 0.098 m/s for 0.027 m^3/s.

Reynolds numbers ranged from 3896 – 85699 when using depth-averaged velocities obtained from the ADV. Shear dispersion factors in the longitudinal direction were plotted against Re for Rhodamine WT dye and each microplastic in Fig. 6a and for each set of fluorometers over depth in Fig. 6b. $\frac{D_x}{Hu_*}$ was largest at lower Re with values reaching up to 13.96 ± 2.19 for PE and smallest also for PE at the depth-averaged velocity of 0.3 m/s with a Re and factor of 69174 and 2.83 ± 0.44 respectively. $\frac{D_x}{Hu_*}$ was similar for Re > 20000 experiencing fully turbulent flow compared to $\frac{D_x}{Hu_*}$ with Re < 7000 which subsequently increased with decreasing Re (Fig. 6a). When averaged across all velocities Rhodamine WT dyes factor was the largest at 6.58 and PEEK's was the smallest at 5.08. When Re > 7000 there was a visible relationship with $\frac{D_x}{Hu_*}$ over depth (Fig. 6b). $\frac{D_x}{Hu_*}$ was largest closer to the channel bed with factors ranging from 6.18 – 7.78 and decreases with distance in the vertical direction, ranging from 4.05 – 6.43 at the surface.

Dimensionless Shields parameters and particle Reynolds numbers were calculated for each polymer with a density > 1 g/cm³ used in this study and plotted against each other using a logarithmic scale in Fig. 7. θ and Re_* in Fig. 7 for PVC at the two slowest velocities were predicted using u_* calculated from ADV velocities due to PVC dropping out, resulting in no measurable concentration data being collected by the fluorometers. All denser than water polymers were below the Shields (1936) and Miller et al. (1977) curves for the slowest two depth-averaged velocities with PVC also being below for 0.101 m/s showing deposition and in agreement with calculated MRs Fig. 7. θ decreases with increasing polymer density, with PMMA ranging from 0.012 – 6.5 and PVC from 0.0016 – 1.88, while Re_* increases with D with PMMA ranging from 0.092 – 2.12 and PVC from 0.070 – 2.4 (Fig. 7). Both θ and Re_* increase with u_* and thus velocity. The green measured polymer zone in Fig. 7 covers the main area on the Shields diagram where polymers with densities ranging from 1.19 – 1.4 g/cm³ within the 20 - 200 µm size class are expected to be located for the range of velocities and smooth channel bed used in this experiment.

3.3 Longitudinal Dispersion

Longitudinal dispersion coefficients for Rhodamine WT dye and each polymer were compared with the *N*-zone and Elder's (1959) models in Fig. 8. The *N*-zone computed a 5.97 factor, similar to Elder's 5.93, and a $\frac{u}{u_*}$ of 20 indicating a smooth channel bed. Elder's (1959) model was not plotted in Fig. 8 because of the equivalent D_x predictions made by the *N*-zone model as a result. The *N*-zone model exhibited reliable predictions when plotted alongside the concentration data. D_x increased linearly with velocity for Rhodamine WT dye and all polymers displayed an R^2 between 0.77 and 0.89. D_x showed greater deviation from the mean at higher velocities and ranged from 0.0012 ± 0.00031 at the slowest depth-averaged velocity of 0.016 m/s to 0.0372 ± 0.0216 at the fastest of 0.361 m/s (Table 2). D_x demonstrated the greatest variability for PVC in line with MR data (§3.1). PMMA and PEEK's D_x (0.0012 ± 0.00031 & 0.0016 ± 0.00033 m²/s) was marginally lower than dye and PE's (0.0021 ± 0.00022 & 0.0024 ± 0.00039 m²/s) at 0.016 m/s, similar to PVC's D_x of 0.00685 ± 0.00233 at 0.169 m/s when compared to dye and PE's (0.011 ± 0.0018 & 0.012 ± 0.0023 m²/s).

Greater dispersion coefficients were recorded for the bottom fluorometers when compared to the middle and top with the difference increasing with velocity (Fig. S6). The longitudinal dispersion increase due to shear was indicative of the velocity profiles displayed in Fig. 5. To measure the average difference between predicted D_x values and measured D_x values for Rhodamine WT dye and each microplastic a root mean square error (RMSE) analysis was undertaken and displayed in Table 3. Polymers were compared to Rhodamine WT dye and the *N*-zone model where all RMSE values were calculated to be less than 0.006. Marginally better values were calculated using Rhodamine WT dye as the predicted value for microplastic dispersion than the *N*-zone model, indicating that dye was an agreeable substitute when used as a proxy for microplastic movement at most velocities present in fluvial systems.

Regressions were plotted for each polymer against Rhodamine WT in Fig. 9 where an R^2 > 0.9 was achieved for each microplastic. Despite zero longitudinal dispersion being recorded for PVC at 0.016 m/s and 0.031 m/s all polymers dispersed similarly to Rhodamine WT dye with PE and PMMA showing the strongest correlation at 0.98 and 0.99 respectively. When the regression was plotted only for polymer velocities with MR percentages > 90, PVC's R^2 was less at 0.86, indicating that the zero dispersion values were slightly skewing the data, although a good R^2 was retrieved regardless (Fig. S7). R^2 for other polymers showed minimal differences if any (Fig. S7). Two-Factor ANOVA's with replication showed no significant difference in D_x over depth or between polymers across all velocities (p-value > 0.05). One-Way ANOVA's comparing each individual polymers D_x against Rhodamine WT dye's D_x also showed no significant difference (p-value > 0.05).

3.4 Image Analysis

With fluorometric techniques unable to accurately quantify PP at all velocities and PVC at slower velocities, a qualitative image analysis was performed for the two density extremes (PP & PVC) at depth-averaged velocities of 0.016 – 0.3 m/s (Mov. S1 – 18). 0.361 m/s was too fast to get any meaningful recordings from the camera and for flows ≥ 0.101 m/s recordings were analysed at 0.25x the normal speed (Mov. S6 – 13). Upon injecting PP and PVC at the beginning of the main flow length of the flume, both polymers were seen to be greatly affected by their respective densities (0.9 – 0.91 g/cm³ and 1.4 g/cm³) for the slower velocities of 0.016 – 0.101 m/s. Large quantities of the injected concentration mass for PP were seen at the water surface for all recorded velocities while the bulk of the of PVC concentration mass settled on the channel bed between 0.016 – 0.101 m/s. PP ascended towards the water surface with little mass remaining at the bottom of the water column, while PVC descended towards the channel bed where it eventually settled with little mass remaining near the top of the water column. Once PP reached the water surface it was subjected to surface tension where it remained. PVC saltated

along the channel bed in straight lines (simulating water flow lines) slowly at 0.101 m/s and faster at 0.169 m/s (Mov. S15 & S16) where large quantities accumulated at the end of the flume (Fig. S8). The bulk of the accumulated PVC mass on the channel bed was reintroduced into the main flow at 0.101 m/s while small amounts saltated along the channel bed and trace amounts at 0.3 m/s. When transported within the water column for flows ≥ 0.101 m/s the bulk of the PVC mass was transported in the longitudinal direction and was difficult to discern from the water. Representative screenshots for PP and PVC at 0.031 m/s are provided in Fig. S9.

4. Discussion

4.1 Transport and Fate

Image analysis revealed virgin PP was expected to become trapped on the water surface over the small timescales used in this study (< 1 h) regardless of velocity. This demonstrates that PP had the greatest mobility of the polymers studied and will likely travel the greatest distances over larger timescales, agreeing with results from Hollein et al. (2019). Considering PP possesses a density very close to that of PE, that is proven to follow the same pathways as neutrally buoyant particles (Abolfathi et al., 2020; Cook et al., 2020; Stride et al., 2023a; Stride et al. 2023b), our results confirm a significant density threshold occurs between 0.9 – 0.94 g/cm^3. More research is needed to confirm whether biofilm formation, aggregation, and an increase in hydrophilicity will cause PP to become neutrally buoyant and sink below the surface after a significant amount of time has passed. Whether this density increase will be significant enough is unclear with Chen et al. (2019) only finding PP density increases of 0.1 g/cm^3 after four weeks for particles with much larger surface areas (0.3 mm thick sheets of 5 x 5 mm).

Determined dispersion characteristics of PE match results from Cook et al. (2020) and Stride et al. (2023a), with PE following the same transport pathways as solutes within the water column, even for the slowest depth-averaged velocity of 0.016 m/s. The denser polymers of

PMMA and PEEK followed the same transport pathways as both solutes and PE for depth-averaged velocities ≥ 0.101 m/s through response curves, MR, and D_x (Figs. 3, 4, 6, & 7). This indicates that within rivers containing velocities ≥ 0.101 m/s, the bulk of spherical polymers containing densities of 0.94 – 1.32 g/cm³ in the 20 - 200 µm size class will remain in the water column and eventually be deposited in marine ecosystems. This conclusion was the same for PVC (1.4 g/cm³) at higher depth-averaged velocities ≥ 0.169 m/s. As displayed in Table 1 and discussed in §1, the majority of microplastics produced within Europe fall within this density range highlighting the applicability of these findings. It is not expected that the different chemical compositions of other polymers would affect their transport and fate over the small timescales used in this study. The two slowest velocities of 0.016 m/s and 0.031 m/s are at the very bottom of the range of mean velocities exhibited by rivers in the environment (Guymer, 2002) and are more indicative to wetlands or ponds. In addition, Khatmullina & Isachenko (2017) and Zhen Wang et al. (2021) concluded that settlement law for various shapes does not significantly differ for cylinders and fragments from that of spherical particles in smaller size ranges for both static and dynamic water conditions. This increases the significance of the results and suggests that once 3D-microplastics (1 - 200 µm in size) with a density ≤ 1.32 g/cm³ enter the water column of a river, most will remain within the water column as long as their density stays below the calculated threshold between 1.32 – 1.4 g/cm³ that causes them to sink at higher velocities between 0.101 m/s and 0.169 m/s. Polymers with densities near 1.4 g/cm³ are still likely to saltate along the channel bed and could be resuspended at these higher velocities as demonstrated in Mov. S15 & S16.

Mixing differences found at slower velocities were highlighted through the ADE's inability to predict accurate response curves presented in Table 2 and lower MR presented in Fig. 4. Although D_x was slightly lower for PMMA and PEEK than dye and PE at 0.016 m/s, and for PVC at 0.169 m/s, it was debateable whether these differences were significant enough to draw a

specific conclusion on D_x alone given the regressions in Fig's. 8 & 9. Combined with MR and routing model R_t^2 results we can conclude a significant difference was found for PMMA, PEEK, and PVC concentrations over depth at these slower velocities. Fig's 8 & 9 do however, support the hypothesis that when moving within the water column, 3D-microplastics exhibit similar dispersion characteristics in the longitudinal direction to that of solutes given a high enough velocity. This was despite the significant difference found in polymer MR across all velocities (p-value < 0.05) because no difference was found in polymer D_x across all velocities (p-value > 0.05). Where polymer mixing differences were found, MRs were influenced by where the particles were located over depth (Fig. S3). Particles located near the water surface were not deposited at the same rates as particles located near the channel bed. This indicates that when polymer density starts to affect microplastic deposition at slower velocities, particles located lower in the water column contain a higher probability of being deposited. Subsequently, this provides valuable information to the limited knowledge of the vertical distribution of microplastics in the water column (Skalska et al., 2020). These results align with Besseling et al. (2017) demonstrating that for the size class of 20 – 200 µm microplastic retention in fluvial systems is strongly associated with polymer density.

In flow domains with slower velocities typical of wetlands and ponds, or dead zones within rivers, microplastics with densities ≥ 1.19 g/cm³ are likely to be deposited in the sediment bed given a long enough exposure time. This was emphasized in Fig. S7 where PVC was deposited in large quantities at a dead zone located at the end of the flume at a depth-averaged velocity of 0.169 m/s (0.012 m³/s) due to dropping out and saltating along the channel bed (Mov. S15 & S16). As a result, an increase in direct microplastic ingestion and respiration may occur for benthic organisms during low flow periods and pelagic organisms during high flow periods. Microplastics have been shown to bioaccumulate within each trophic level (Miller et al., 2020) and results of previous studies have indicated that microplastic exposure may strongly correlate with toxicity

(Kim & An, 2020). However, these microplastic “hot spots” can be used for microplastic remediation through collecting and treating denser microplastics, thus preventing them from being resuspended in the water column and as a result the environment. River loads exhibit high degrees of variation meaning that microplastics deposited in these hot spots will likely be resuspended during high flows in line with results from Lu et al. (2023). Precipitation events in an urban part of the Rhone catchment were shown to increase plastic concentrations up to 150 times (Faure et al., 2015). Therefore, management strategies should be in place to identify these hot spots with slower velocities or construct them as designated water treatment areas. Proven microplastic collection techniques can then be implemented to reduce resuspension during high flows. Many other factors such as aggregation, biofilm formation, and sediment composition, along with microplastic shape and size (discussed in §1) need to be quantified to determine which are the most dominant and thus important in determining microplastic fate.

Waldschläger et al.’s (2022) review highlighted the need for quantifying the dynamic behaviour of microplastics and conducting flume experiments determining shear stress thresholds for microplastic resuspension. Fig. 7 is the first instance of calculating shear stress thresholds for microplastic resuspension that covers a range of polymer types and densities. The Shields diagram supports our findings in that PMMA and PEEK were below Shields (1936) and Miller et al. (1977) curves for velocities ≤ 0.031 m/s and for PVC ≤ 0.101 m/s. Fig. 7 matched against our experimental data confirms that the majority of microplastics with densities ≤ 1.32 g/cm^3 will either be suspended in the water column or floating at the surface at velocities ≥ 0.101 m/s. Marginally reduced MRs were detected for PVC at 0.169 m/s, demonstrating a potential discrepancy between the expected deposition of PVC due to θ being above both the Shields (1936) and Miller et al. (1977) curves. PVCs saltating at 0.169 m/s or the true velocity threshold of PVC deposition being between 0.101 – 0.169 m/s are likely the contributing factors. Even if a significant portion is depositing in the channel bed and not detected by the fluorometers, this portion is still in motion

and thus above the Shields (1936) and Miller et al. (1977) curves. As Shields parameters analyse the onset of motion, with studies normally starting with particles on the channel bed, it is difficult to determine whether microplastics are transported significantly earlier than sediments as suggested by Waldschläger & Schüttrumpf (2019). With large portions still in motion for PMMA and PEEK (MR = 73 – 87 %), over the short distance of the flume, whilst being below the Shields (1936) and Miller et al., (1977) curves there is evidence to support this. Overall, our experiment indicates that Shields parameters can produce good first predictions of polymer shear stress thresholds and provide a reasonable first estimate of microplastic fate based on density and D.

It is expected for the 20 – 200 µm size class that approximate critical motion or resuspension thresholds will occur between θ values of approximately 0.51 for the lightest polymers > 1 g/cm³ at 1.05 g/cm³ (PS) and 0.09 for the densest most common polymers around 1.4 g/cm³ (PVC) when predicting θ utilizing a $\frac{u}{u_*}$ of 20 and extreme values of D (20 µm for PS and 200 µm for PVC). For the smooth bed in this experiment these corresponded to approximate depth-averaged velocities of 0.046 – 0.17 m/s. Given that PSs density is close to that of water there is a chance that most of the concentration mass will remain in the water column similar to PE across all velocities used in this study, preventing deposition. Apparent Re_* increases with density in Fig. 7 are due to slightly larger D values for the denser polymers chosen in this study. This is because density is not used to calculate Re_* in Eq. (9) and obtaining multiple polymers with the exact same D for tests is notoriously difficult. The predicted polymer zone indicates that microplastics may produce lower Re_* than expected from some natural sediments.

4.2 Mixing and Fluorometric Fundamentals

The ADE model provided robust predictions with reliable accuracies of R_t^2 > 0.95 showing that simple routing models can be used to predict microplastic mixing for 3D-spheres ≤ 200 µm in size. The accuracy of the ADE routing model was ultimately dependent on the density of the microplastic and the corresponding velocity in the water column (Table 2). Response curves can

be accurately predicted within the water column for PE with depth-averaged velocities ≥ 0.016 m/s, PMMA and PEEK ≥ 0.101 m/s, and PVC ≥ 0.169 m/s. With the PVC used in this experiment containing the largest diameter of the polymers tested (63 – 150 µm) the signal fluctuation of the optical sensor in the fluorometers was close to reaching the upper size limit at faster velocities to accurately quantify solid particle movement. This was indicated through PVC's larger confidence intervals in the concentration data compared to the other polymers and therefore it is not recommended that studies utilize fluorometric techniques for solid particles > 150 µm in diameter. The ADE R_t^2 of 0.871 for PVC at a depth-averaged velocity of 0.3 m/s (Table 2) is an example of signal fluctuation potentially influencing results. With Boos et al. (2021) utilizing fluorometric techniques for microplastics 1-10 µm in diameter, we can confirm stained particles with diameters of 1 – 150 µm can be accurately traced using fluorometric techniques (see Fig. 3). Fluorometric quantification for microplastics worked best for smaller microplastic sizes and it is likely that microplastics < 1 µm can be traced but a lower size limit for fluorometric detection still needs to be quantified.

Low RMSE values and matching regressions in Fig. 8 demonstrate the applicability of both Elder's (1959) and Chikwendu's (1986) *N*-zone model for predicting microplastic dispersion coefficients. Simply analysing velocities over depth can then reasonably predict the dispersion of 3D-microplastics for polymers with densities ranging from 0.94 – 1.4 g/cm³ over short timescales in fluvial environments when velocities are high enough and polymers are well-mixed over depth. We have determined this to be a above depth-averaged velocity thresholds ≥ 0.016 m/s for polymers of a near-neutral buoyancy, ≥ 0.101 m/s for polymers with densities ranging from 1.19 – 1.32 g/cm³, and ≥ 0.169 m/s for polymers with densities near 1.4 g/cm³.Rhodamine WT dyes mean shear dispersion factor of 6.58 is in line with Elder's (1959) 5.93 when including shear dispersion initiated by the flume walls, thus validating dispersion results against proven theoretical means. PE displayed a similar average dispersion factor of 6.17 and PMMA, PEEK, and PVC

ranged between 5.16 – 5.35. This was due to larger shear dispersion factors found at $Re \leq 7000$ in Figs. 6a & 6b which were less for PMMA, PEEK, and PVC due to not being well-mixed over depth (Figs. 4 & S3) and lower D_x values (Table 2) because of their higher densities. Therefore, Elder's (1959) 5.93 shear dispersion factor is an excellent guideline for mixing studies, but it should be noted that higher factors are expected at lower Re as the flow becomes more laminar and less turbulent for solid particles as well as solutes. Fig. 6b also showed that shear dispersion and therefore D_x was affected by where the fluorometer was positioned over depth. As distance increased from the channel bed, dispersion due to shear decreased and smaller D_x values were produced as a result. This was likely due to the relative effects turbulence generated from the channel bed had on the flow in relation to the turbulence produced by differential advection, illustrated in the Fig. 5 velocity profiles. Future studies employing fluorometric techniques should consider the influence of particle size, Re, and distance from the channel bed when performing experiments.

5. Conclusion

The effects of density on the transport and fate of microplastics in open channel flows were comprehensively explored for 3D-polymers within the 20 – 200 μm size class. The boundaries of fluorometric and staining techniques for solid particles within the water column of fluvial environments required polymer densities to be > 0.9 g/cm³ and their particle size to be < 150 μm for accurate quantification. Critical suspension and deposition thresholds using solute transport techniques agreed with the classical Shields (1936) methodology (Fig. 7). Reliable model predictions for the ADE and *N*-zone were confirmed for specific depth-averaged velocities related to each polymer (see §4.2). In the vast majority of conditions tested microplastics exhibited similar transport characteristics to solutes, where solute transport techniques are more applicable to determine microplastic fate. However, microplastic deposition and resuspension was strongly

associated with polymer density for critical velocity thresholds ≤ 0.101 m/s, where particle transport techniques are more applicable.

For this class of microplastics, in freshwater systems containing velocities that are low enough for particle density to become the dominant force (≤ 0.031 m/s), concentrations of denser than water microplastics will be momentarily or permanently deposited in channel beds. This may increase direct microplastic exposure for benthic organisms during low flow periods and pelagic organisms during high flow periods. The velocity threshold for microplastics with densities 1.19 g/cm³ ≤ 1.32 g/cm³ was ≤ 0.031 m/s (Re ≤ 7254) and for polymers with a density nearer to 1.4 g/cm³ ≤ 0.101 m/s (Re ≤ 24018) demonstrating a density threshold occurs between 1.32 – 1.4 g/cm³ where faster velocities are required for microplastic suspension. When polymer density starts to affect microplastic deposition at slower velocities, particles located lower in the water column were found to contain a higher probability of being deposited. For the same class of microplastics, polymers with densities ≤ 0.9 g/cm³ will ascend to the surface regardless of velocity making them the most mobile. This data is the first to provide specific microplastic suspension and deposition thresholds based on river velocity and polymer density, making a key contribution to research predicting microplastic fate and organismal exposure. It is important to recognize this study is limited to open channels and a specific class of microplastics over short timescales < 1 h. The effects microplastic density within other microplastic classes and flow domains over timescales long enough for polymer degradation to occur need to be researched in future studies. The resulting effects on polymer density can then be compared to the results in this study to see if the same determined density and velocity thresholds apply.

6. Acknowledgements

Funding was provided by the Natural Environmental Research Council (NERC) and The Central England NERC Training Alliance (CENTA). We also acknowledge our Civil Engineering Technician Joel Whittle for help in setting up the experiment.

NERC grant NE/S007350/1 (243303, BS)

7. Declarations

We confirm that none of the material has been published or is under consideration for publication elsewhere, and we have no conflicts of interest to declare. All data used in the analysis will be made available on the online repository of the University of Warwick, WRAP.

8. References

Abolfathi, S., Cook, S., Yeganeh-Bakhtiary, A., Borzooei, S., & Pearson, J. (2020). Microplastics Transport and Mixing Mechanisms in the Nearshore Region. *Coastal Engineering Proceedings*, *36v*, 63. https://doi.org/10.9753/icce.v36v.papers.63

Arnaud-Fassetta, G., Quisserne, D., & Antonelli, C. (2003). Downstream grain-size distribution of surficial bed material and its hydro-geomorphological significance in a large and regulated river: the Rhône River in its delta area (France). *Géomorphologie Relief Processus Environnement*, *9*(1), 33–49. https://doi.org/10.3406/morfo.2003.1164

Ballent, A., Pando, S., Purser, A., Juliano, M. F., & Thomsen, L. (2013). Modelled transport of benthic marine microplastic pollution in the Nazaré Canyon. *Biogeosciences*, *10*(12), 7957–7970. https://doi.org/10.5194/bg-10-7957-2013

Barnes, D. K. A., Galgani, F., Thompson, R. C., & Barlaz, M. (2009). Accumulation and fragmentation of plastic debris in global environments. *Philosophical Transactions of the Royal Society B: Biological Sciences*, *364*(1526), 1985–1998. https://doi.org/10.1098/rstb.2008.0205

Besseling, E., Quik, J. T. K., Sun, M., & Koelmans, A. A. (2017). Fate of nano- and microplastic in freshwater systems: A modeling study. *Environmental Pollution*, *220*(1), 540–548. https://doi.org/10.1016/j.envpol.2016.10.001

Boos, J. P., Gilfedder, B. S., & Frei, S. (2021). Tracking Microplastics Across the Streambed Interface: Using Laser-Induced-Fluorescence to Quantitatively Analyze Microplastic Transport in an Experimental Flume. *Water Resources Research*, *57*(12), 1–10. https://doi.org/10.1029/2021WR031064

British Plastics Federation. (2023). Thermoplastics. Retrieved 18th May 2023 from: https://www.bpf.co.uk/plastipedia/polymers/polymer-thermoplastics.aspx#polyesters

Chamas, A., Moon, H., Zheng, J., Qiu, Y., Tabassum, T., Jang, J. H., Abu-Omar, M., Scott, S. L., & Suh, S. (2020). Degradation Rates of Plastics in the Environment. *ACS Sustainable Chemistry and Engineering*, *8*(9), 3494–3511. https://doi.org/10.1021/acssuschemeng.9b06635

Chen, X., Xiong, X., Jiang, X., Shi, H., & Wu, C. (2019). Chemosphere Sinking of floating plastic debris caused by bio fi lm development in a freshwater lake. *Chemosphere, 222*(5), 856–864. https://doi.org/10.1016/j.chemosphere.2019.02.015

Chikwendu, S. C. (1986). Calculation of longitudinal shear dispersivity using an n-zone model as n-> ∞. *Journal of Fluid Mechanics*, *167*, 19–30. https://doi.org/10.1017/S0022112086002707

Cook, S., Chan, H. L., Abolfathi, S., Bending, G. D., Schäfer, H., & Pearson, J. M. (2020). Longitudinal dispersion of microplastics in aquatic flows using fluorometric techniques. *Water Research*, *170*(3), 115337. https://doi.org/10.1016/j.watres.2019.115337

Coyle, R., Hardiman, G., & Driscoll, K. O. (2020). Microplastics in the marine environment: A review of their sources, distribution processes, uptake and exchange in ecosystems. Case *Studies in Chemical and Environmental Engineering, 2*(4), 100010. https://doi.org/10.1016/j.cscee.2020.10001

de Haan, W. P., Sanchez-Vidal, A., & Canals, M. (2019). Floating microplastics and aggregate

formation in the Western Mediterranean Sea. *Marine Pollution Bulletin*, *140*(2), 523–535. https://doi.org/10.1016/j.marpolbul.2019.01.053

Do, A. T. N., Ha, Y., & Kwon, J. H. (2022). Leaching of microplastic-associated additives in aquatic environments: A critical review. *Environmental Pollution, 305*(3), 119258. https://doi.org/10.1016/j.envpol.2022.119258

Eerkes-Medrano, D., Thompson, R. C., & Aldridge, D. C. (2015). Microplastics in freshwater systems: A review of the emerging threats, identification of knowledge gaps and prioritisation of research needs. *Water Research*, *75*(5), 63–82. https://doi.org/10.1016/j.watres.2015.02.012

Elder, J. W. (1959). The dispersion of marked fluid in turbulent shear flow. *Journal of Fluid Mechanics*, *5*(4), 544. https://doi.org/10.1017/S0022112059000374

Faure F, Demars C, Wieser O et al (2015) Plastic pollution in Swiss surface waters: nature and concentrations, interaction with pollutants. *Environmental Chemistry 12*(5), 582–591

Fischer, H. (1966). Longitudinal Dispersion in Laboratory and Natural Streams. *Technical Report. Keck Laboratory of Hydraulic and Water Resources, California Institution of Technology, Pasadena, California*.

Frias, J. P. G. L., & Nash, R. (2019). Microplastics: Finding a consensus on the definition. *Marine Pollution Bulletin*, *138*(9), 145–147. https://doi.org/10.1016/j.marpolbul.2018.11.022

Goring, D. G., & Nikora, V. I. (2002). Despiking Acoustic Doppler Velocimeter Data. *Journal of Hydraulic Engineering*, *128*(1), 117–126. https://doi.org/10.1061/(asce)0733-9429(2002)128:1(117)

Guymer, I., & Environment Agency. (2002). *A national database of travel time, dispersion and methodologies for the protection of river abstractions.*

Guymer, I., & Stovin, V. R. (2011). One-Dimensional Mixing Model for Surcharged Manholes. *Journal of Hydraulic Engineering*, *137*(10), 1160–1172. https://doi.org/10.1061/(asce)hy.1943-7900.0000422

He, B., Smith, M., Egodawatta, P., Ayoko, G. A., Rintoul, L., & Goonetilleke, A. (2021). Dispersal and transport of microplastics in river sediments. *Environmental Pollution, 279*(6), 116884. https://doi.org/10.1016/j.envpol.2021.116884

He, S., Jia, M., Xiang, Y., Song, B., Xiong, W., Cao, J., Peng, H., Yang, Y., Wang, W., Yang, Z., & Zeng, G. (2022). Biofilm on microplastics in aqueous environment: Physicochemical properties and environmental implications. *Journal of Hazardous Materials, 424*(2), 127286. https://doi.org/10.1016/j.jhazmat.2021.127286

Hoellein, T. J., Shogren, A. J., Tank, J. L., Risteca, P., & Kelly, J. J. (2019). Microplastic deposition velocity in streams follows patterns for naturally occurring allochthonous particles. *Scientific Reports*, *9*(1), 1–11. https://doi.org/10.1038/s41598-019-40126-3

Jobson, H.E., & Sayre, W.W. (1970). Vertical Transfer in Open Channel Flow. *Journal of Hydraulic Engineering, 96*(3), 703-724

Khatmullina, L., & Isachenko, I. (2017). Settling velocity of microplastic particles of regular shapes. *Marine Pollution Bulletin*, *114*(2), 871–880. https://doi.org/10.1016/j.marpolbul.2016.11.024

Kim, S. W., & An, Y. (2020). Edible size of polyethylene microplastics and their effects on springtail. *Environmental Pollution*, *266*(11), 115255. https://doi.org/10.1016/j.envpol.2020.115255

Kooi, M., Besseling, E., Kroeze, C., van Wezel, A. P., & Koelmans, A. A. (2018). Erratum to: Modeling the Fate and Transport of Plastic Debris in Freshwaters: Review and Guidance. *The Handbook of Environmental Chemistry, 58*(1). https://doi.org/10.1007/978-3-319-

61615-5_14

Kumar, R., Sharma, P., Verma, A., Jha, P. K., Singh, P., Gupta, P. K., Chandra, R., & Vara Prasad, P. V. (2021). Effect of physical characteristics and hydrodynamic conditions on transport and deposition of microplastics in riverine ecosystem. *Water, 13*(19), 2710. https://doi.org/10.3390/w13192710

Lagarde, F., Olivier, O., Zanella, M., Daniel, P., Hiard, S., & Caruso, A. (2016). Microplastic interactions with freshwater microalgae: Hetero-aggregation and changes in plastic density appear strongly dependent on polymer type. *Environmental Pollution*, *215*(8), 331–339. https://doi.org/10.1016/j.envpol.2016.05.006

Lobelle, D., & Cunliffe, M. (2011). Early microbial biofilm formation on marine plastic debris. *Marine Pollution Bulletin*, *62*(1), 197–200. https://doi.org/10.1016/j.marpolbul.2010.10.013

Lu, X., Wang, X., Liu, X., & Singh, V. P. (2023). Dispersal and transport of microplastic particles under different flow conditions in riverine ecosystem. *Journal of Hazardous Materials*, *442*(1), 130033. https://doi.org/10.1016/j.jhazmat.2022.130033

Mendrik, F., Fernández, R., Hackney, C. R., Waller, C., & Parsons, D. R. (2023). Non-buoyant microplastic settling velocity varies with biofilm growth and ambient water salinity. *Communications Earth and Environment*, *4*(1), 1–9. https://doi.org/10.1038/s43247-023-00690-z

Miller, M. E., Hamann, M., & Kroon, F. J. (2020). Bioaccumulation and biomagnification of microplastics in marine organisms: A review and meta-analysis of current data. *PLoS ONE*, *15*(10), 1–25. https://doi.org/10.1371/journal.pone.0240792

Nguyen, T. H., Tang, F. H. M., & Maggi, F. (2020). Sinking of microbial-associated microplastics in natural waters. *PLoS ONE*, *15*(2), 1–20. https://doi.org/10.1371/journal.pone.0228209

Nizzetto, L., Bussi, G., Futter, M. N., Butterfield, D., & Whitehead, P. G. (2016). A theoretical assessment of microplastic transport in river catchments and their retention by soils and river sediments. *Environmental Science: Processes and Impacts*, *18*(8), 1050–1059. https://doi.org/10.1039/c6em00206d

Onink, V., Kaandorp, M. L. A., Van Sebille, E., & Laufkötter, C. (2022). Influence of Particle Size and Fragmentation on Large-Scale Microplastic Transport in the Mediterranean Sea. *Environmental Science and Technology*, *56*(22), 15528–15540. https://doi.org/10.1021/acs.est.2c03363

Plastics Europe. (2022). Plastics the Facts 2022. 1-81. Retrieved 18th May 2023 from: https://plasticseurope.org/wp-content/uploads/2022/10/PE-PLASTICS-THE-FACTS_V7-Tue_19-10-1.pdf

Pramanik, B. K., Pramanik, S. K., & Monira, S. (2021). Understanding the fragmentation of microplastics into nano-plastics and removal of nano/microplastics from wastewater using membrane, air flotation and nano-ferrofluid processes. *Chemosphere*, *282*(10), 131053. https://doi.org/10.1016/j.chemosphere.2021.131053

Rehse, S., Kloas, W., & Zarfl, C. (2016). Short-term exposure with high concentrations of pristine microplastic particles leads to immobilisation of Daphnia magna. *Chemosphere*, *153*(6), 91–99. https://doi.org/10.1016/j.chemosphere.2016.02.133

Rutherford, J.C. (1994). River Mixing. *John Wiley and Sons, New York*

Sana, S. S., Dogiparthi, L. K., Gangadhar, L., Chakravorty, A., & Abhishek, N. (2020). Effects of microplastics and nanoplastics on marine environment and human health. *Environmental Science and Pollution Research*, *27*(36), 44743–44756. https://doi.org/10.1007/s11356-020-10573-x

Skalska, K., Ockelford, A., Ebdon, J. E., & Cundy, A. B. (2020). Riverine microplastics: Behaviour, spatio-temporal variability, and recommendations for standardised sampling and monitoring. *Journal of Water Process Engineering*, *38*(12), 101600. https://doi.org/10.1016/j.jwpe.2020.101600

Stride, B., Abolfathi, S., Odara, M. G. N., Bending, G. D., & Pearson, J. (2023a). Modeling Microplastic and Solute Transport in Vegetated Flows. *Water Resources Research, 59*(5), e2023WR034653. https://doi.org/10.1029/2023WR034653

Stride, B., Dykes, C., Abolfathi, S., Jimoh, M., Bending, G. D., & Pearson, J. (2023b). Microplastic transport dynamics in surcharging and overflowing manholes. Science of The Total Environment. Volume 899, 165683. https://doi.org/10.1016/j.scitotenv.2023.165683

Suaria, G., & Aliani, S. (2014). Floating debris in the Mediterranean Sea. *Marine Pollution Bulletin*, *86*(1–2), 494–504. https://doi.org/10.1016/j.marpolbul.2014.06.025

Talbot, R., & Chang, H. (2022). Microplastics in freshwater: A global review of factors affecting spatial and temporal variations. *Environmental Pollution*, *292*(1), 118393. https://doi.org/10.1016/j.envpol.2021.118393

Taylor, G. (1954). The dispersion of matter in turbulent flow through a pipe. *Proceedings of the Royal Society of London. Series A. Mathematical and Physical Sciences*, *223*(1155), 446–468. https://doi.org/10.1098/rspa.1954.0130

Waldschläger, K., Brückner, M. Z. M., Carney Almroth, B., Hackney, C. R., Adyel, T. M., Alimi, O. S., Belontz, S. L., Cowger, W., Doyle, D., Gray, A., Kane, I., Kooi, M., Kramer, M., Lechthaler, S., Michie, L., Nordam, T., Pohl, F., Russell, C., Thit, A., … Wu, N. (2022). Learning from natural sediments to tackle microplastics challenges: A multidisciplinary perspective. *Earth-Science Reviews*, *228*(5), 104021. https://doi.org/10.1016/j.earscirev.2022.104021

Waldschläger, K., & Schüttrumpf, H. (2019). Effects of Particle Properties on the Settling and Rise Velocities of Microplastics in Freshwater under Laboratory Conditions. *Environmental Science and Technology*, *53*(4), 1958–1966. https://doi.org/10.1021/acs.est.8b06794

Wang, X., Bolan, N., Tsang, D. C. W., Sarkar, B., Bradney, L., & Li, Y. (2021). A review of microplastics aggregation in aquatic environment: Influence factors, analytical methods, and environmental implications. *Journal of Hazardous Materials*, *402*(1), 123496. https://doi.org/10.1016/j.jhazmat.2020.123496

Wang, Z., Dou, M., Ren, P., Sun, B., Jia, R., & Zhou, Y. (2021). Settling velocity of irregularly shaped microplastics under steady and dynamic flow conditions. *Environmental Science and Pollution Research, 28*(44), 62116–62132. https://doi.org/10.1007/s11356-021-14654-3

Whitehead, P. G., Bussi, G., Hughes, J. M. R., Castro-Castellon, A. T., Norling, M. D., Jeffers, E. S., Rampley, C. P. N., Read, D. S., & Horton, A. A. (2021). Modelling Microplastics in the River Thames: Sources, Sinks and Policy Implications. *Water*, *13*(6), 861. https://doi.org/10.3390/w13060861

Yuan, Z., Nag, R., & Cummins, E. (2022). Human health concerns regarding microplastics in the aquatic environment - From marine to food systems. *Science of the Total Environment*, *823*(6), 153730. https://doi.org/10.1016/j.scitotenv.2022.153730

Ziccardi, L. M., Edgington, A., Hentz, K., Kulacki, K. J., & Kane Driscoll, S. (2016). Microplastics as vectors for bioaccumulation of hydrophobic organic chemicals in the marine environment: A state-of-the-science review. *Environmental Toxicology and Chemistry*, *35*(7), 1667–1676. https://doi.org/10.1002/etc.3461

Tables

Table 1. Plastic polymer production, demand, and density. Data provided by Plastics Europe (2022) and the British Plastics Federation

Polymer Type	Production Demand (%)	Metric Tonnes (Mt)	Density (g/cm³)
Polyethylene (PE) *high-density, medium-density, low-density, linear low-density*	29.4	14.8	0.917 - 0.965
Polyethylene terephthalate (PET)	7.9	4	1.3 - 1.4
Polypropylene (PP)	19.8	10	0.895 – 0.92
Polystyrene (PS)	6.2	1.5	0.96 - 1.06
Polyurethane (PUR) *solid*	8.2	4.1	1.2
Polyvinyl Chloride (PVC)	10.3	5.2	1.38 - 1.4
Total	81.8	39.6	N/A

Table 2. Summary of experimental flow conditions and parameters. Where n is the number of replicates, Q is the initial discharge in the pipe, Re is the Reynolds number, u_* is the bed shear velocity

					D_x (m²/s)							R_t^2 (ADE/ADV)				
n (m³/s)	Q (m³/s)	Depth-Averaged Velocity (m/s)	Re	u_*	Dye	PE	PMMA	PEEK	PVC	Elder	N-zone	Dye	PE	PMMA	PEEK	PVC
4	0.001	0.016	3896	0.008	0.021	0.024	0.012	0.016	N/A	0.012	0.012	0.987	0.960	0.515	0.268	N/A
4	0.002	0.031	7254	0.015	0.029	0.021	0.016	0.023	N/A	0.023	0.023	0.991	0.989	0.898	0.904	N/A
4	0.007	0.101	24018	0.051	0.069	0.070	0.072	0.059	0.055	0.076	0.076	0.986	0.983	0.968	0.994	0.000
4	0.012	0.169	40100	0.085	0.107	0.115	0.114	0.111	0.069	0.126	0.126	0.983	0.966	0.970	0.976	0.965

4	0.017	0.235	557066	0.0117	0.0111	0.0097	0.0105	0.0115	0.0192	0.0175	0.0175	0.995	0.974	0.984	0.978	0.956
4	0.022	0.300	711866	0.0150	0.0130	0.0103	0.0123	0.0108	0.0154	0.0224	0.0224	0.978	0.959	0.993	0.952	0.871
4	0.027	0.361	856999	0.0181	0.0277	0.0228	0.0318	0.0183	0.0372	0.0268	0.0270	0.993	0.930	0.98	0.976	0.963

Table 3. Root mean square error (RMSE) comparison between microplastic polymers, Rhodamine WT dye and the N-zone model

	RMSE				
Comparison	**Dye**	**PE**	**PMMA**	**PEEK**	**PVC**
Dye	N/A	0.00223	0.00170	0.00369	0.00522
N-zone	0.00441	0.00570	0.00503	0.00599	0.00536

Figures

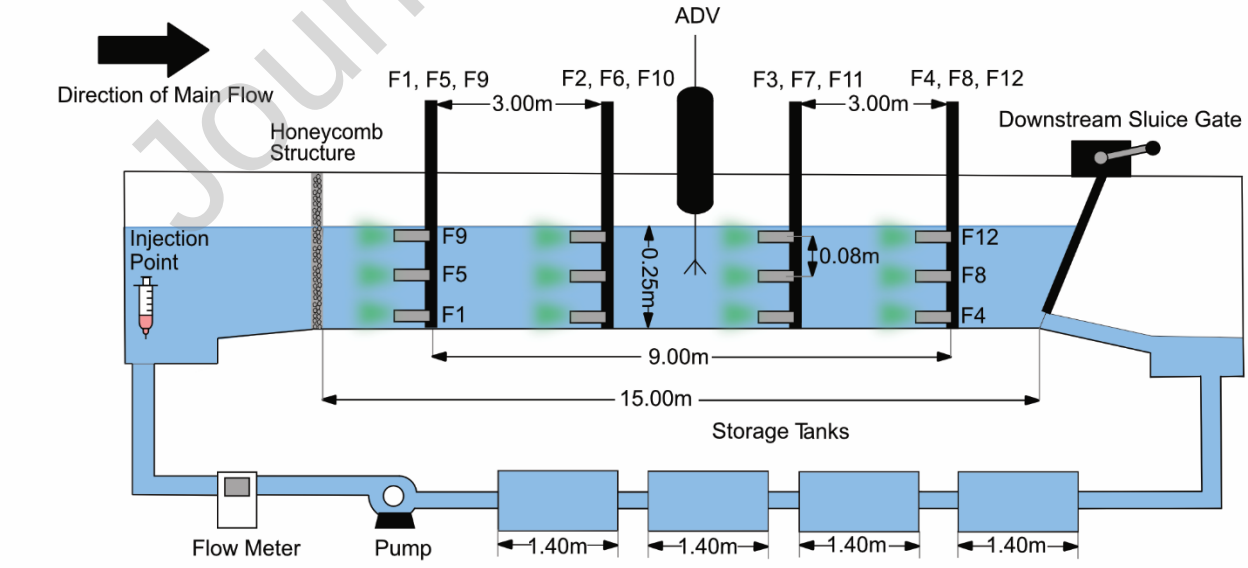

Fig. 1. 2D Laboratory flume diagram (not to scale)

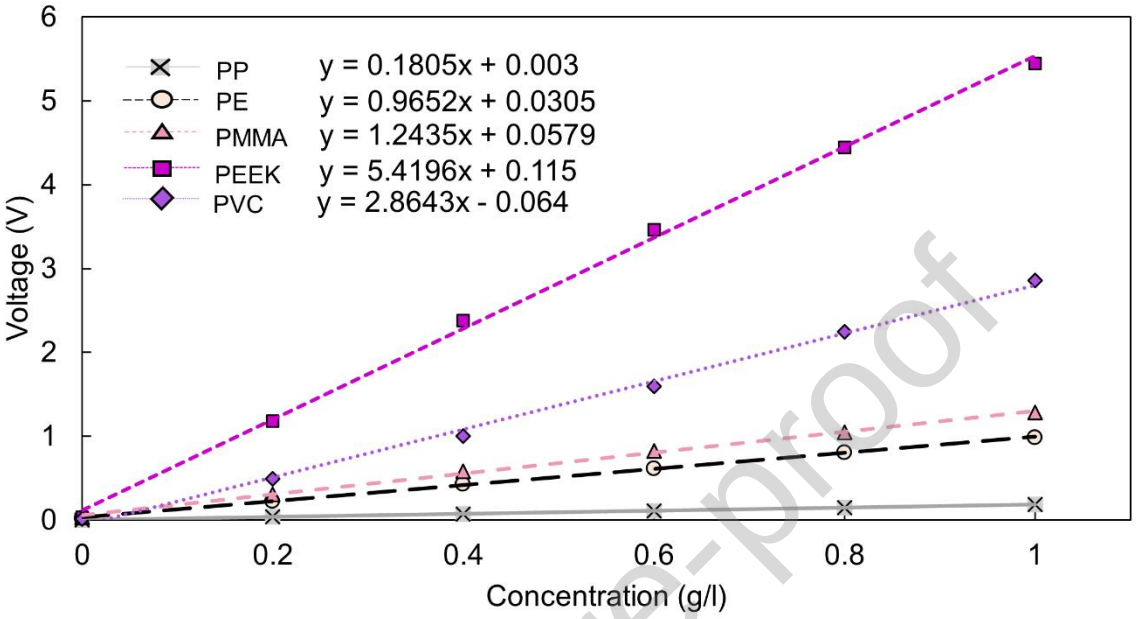

Fig. 2. Different polymer gradients for the microplastic staining process

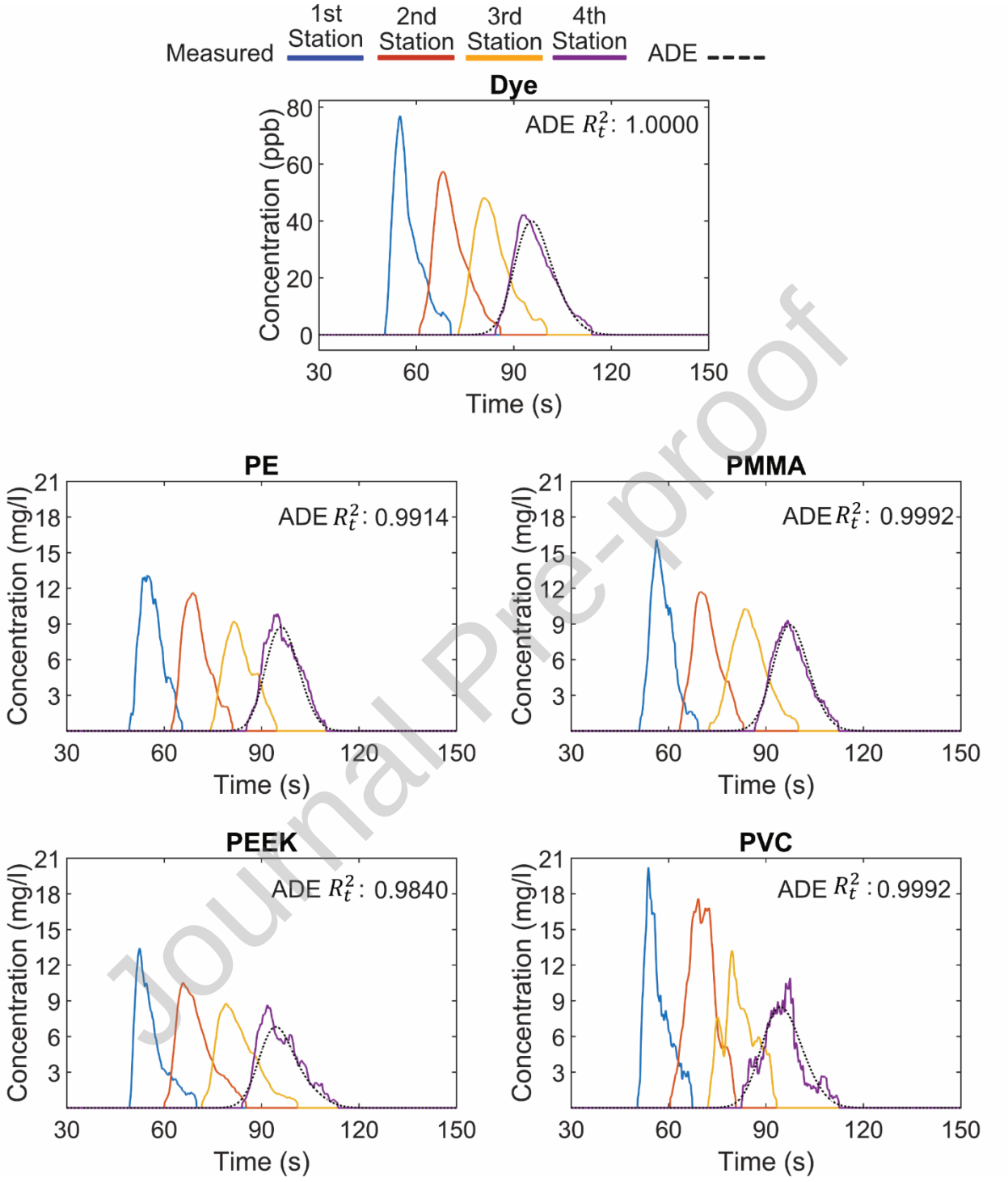

Fig. 3. Measured and predicted response curves for dye and microplastics at 0.235 m/s.

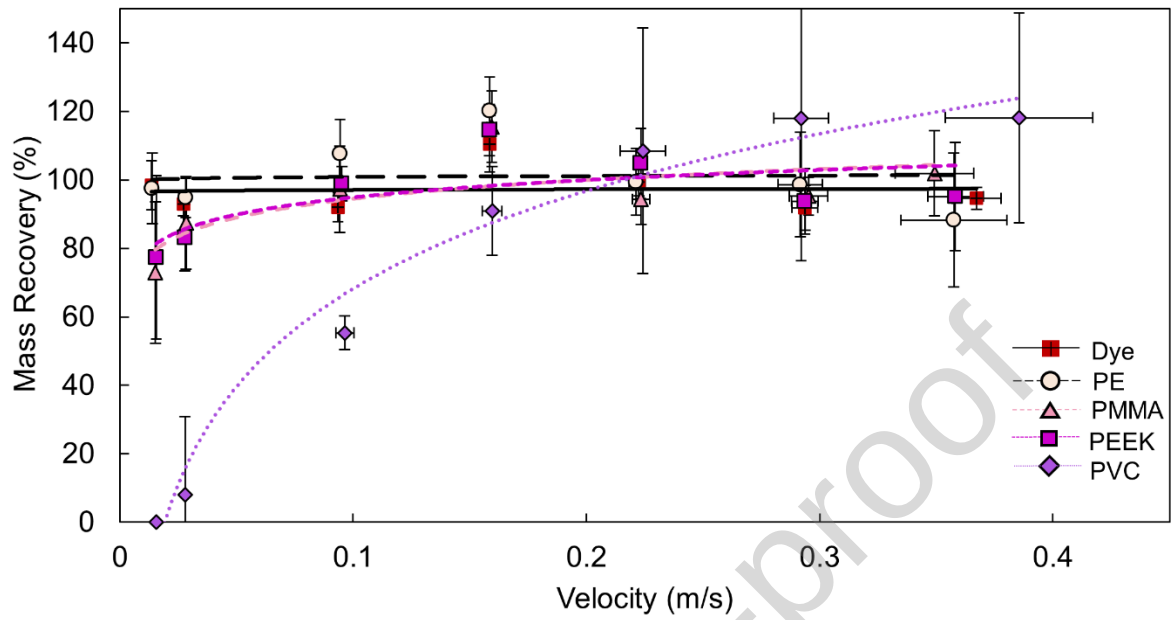

Fig. 4. Mean MR for each microplastic and Rhodamine WT dye (± 95 % confidence intervals)

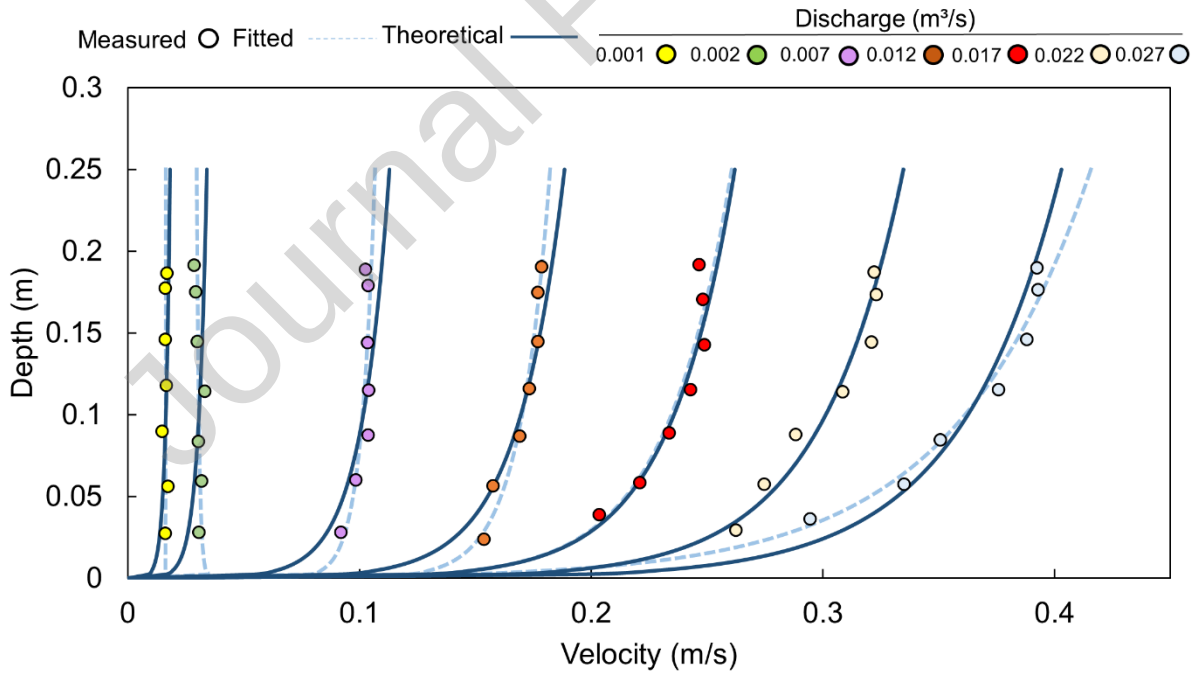

Fig. 5. Measured mean velocities for each ADV setup over the vertical, plus fitted and theoretical velocity profiles for all discharges

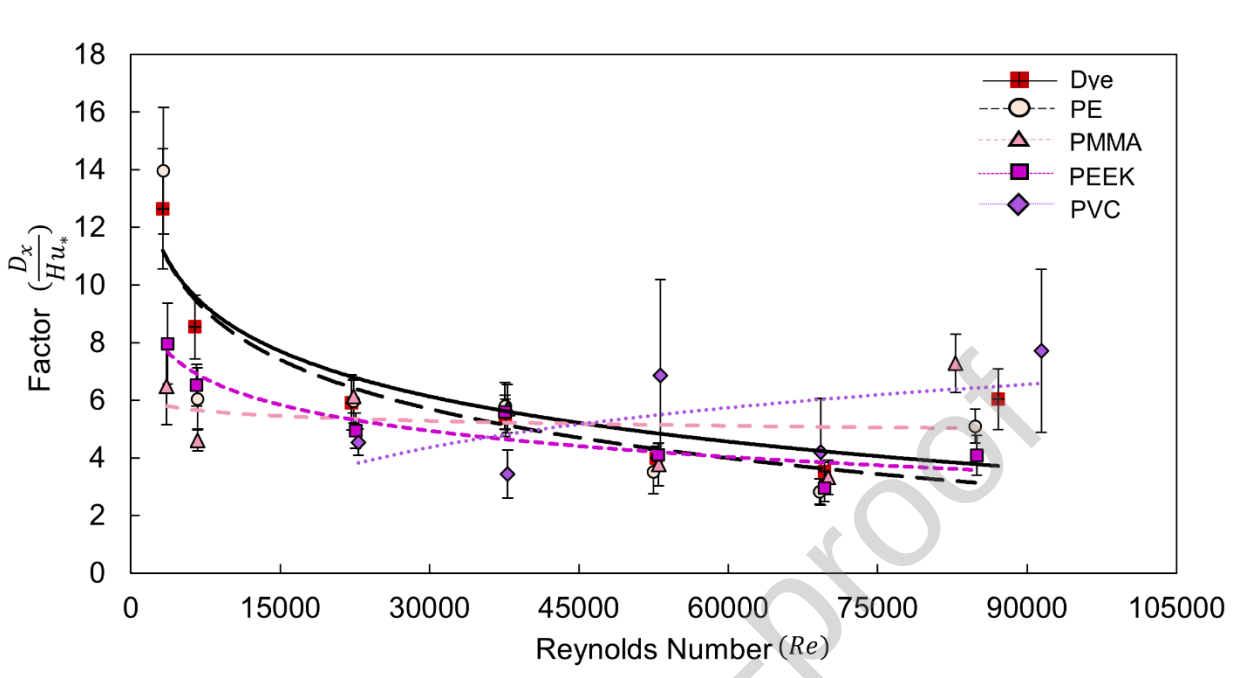

Fig. 6a. Reynolds number vs factor for all microplastics and Rhodamine WT dye (± 95 % confidence intervals)

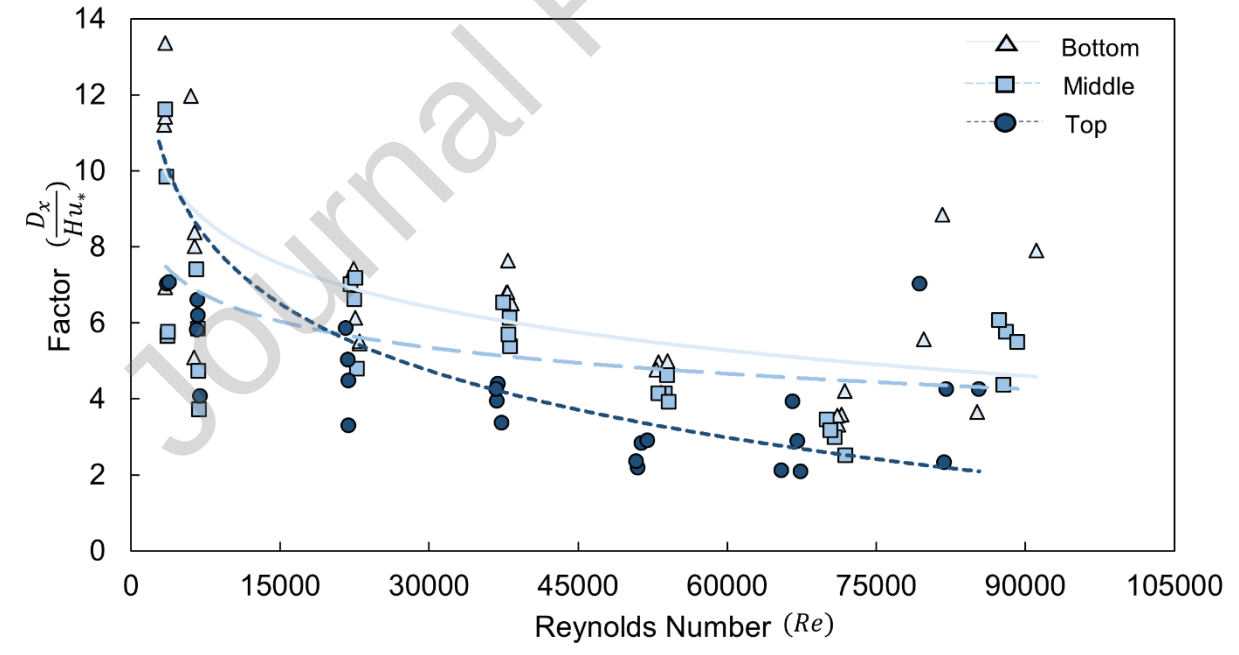

Fig. 6b. Reynolds number vs factor for all microplastics and Rhodamine WT dye when separated over depth (Top vs Middle vs Bottom)

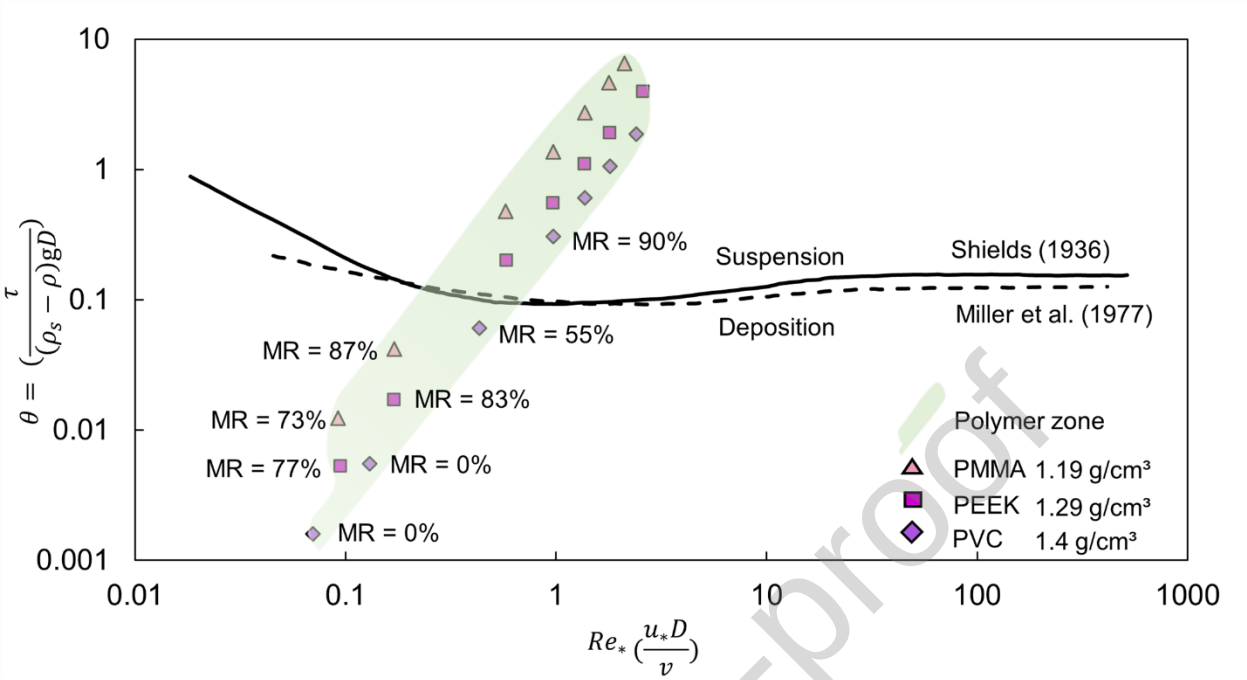

Fig. 7. Shields diagram including associated MRs for microplastic polymers used in this experiment. MRs that are not labelled are near 100 %. Adapted from Arnaud-Fassetta et al. (2003).

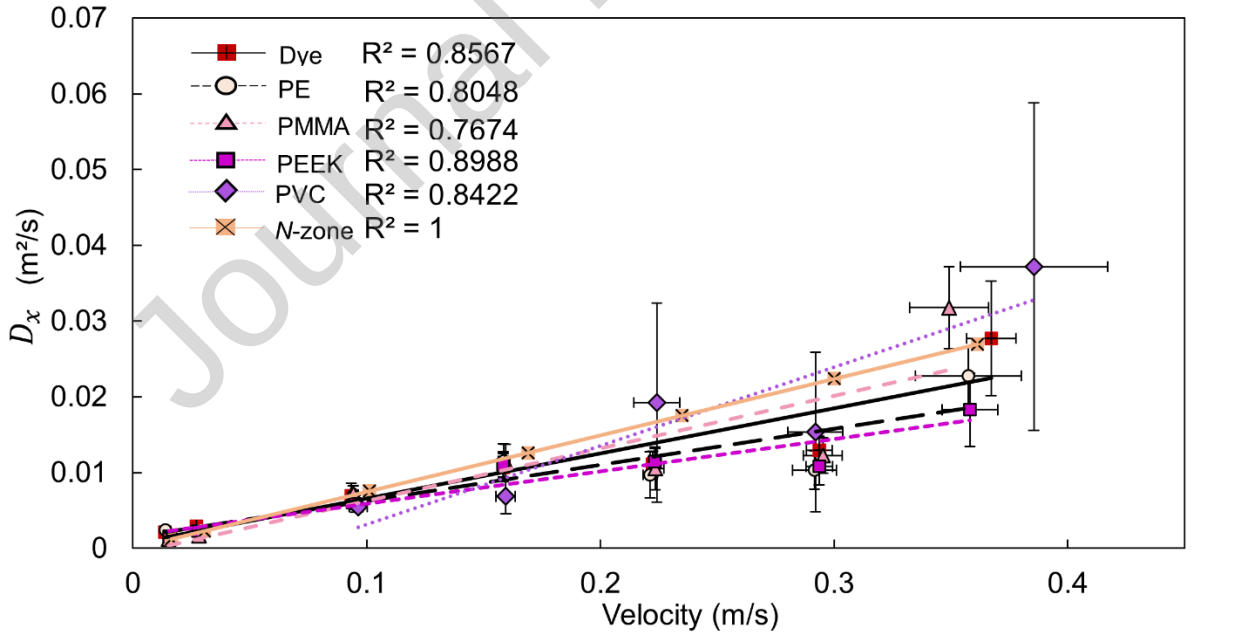

Fig. 8. Calculated and modelled longitudinal dispersion coefficients for each microplastic and Rhodamine WT dye against velocity (± 95 % confidence intervals)

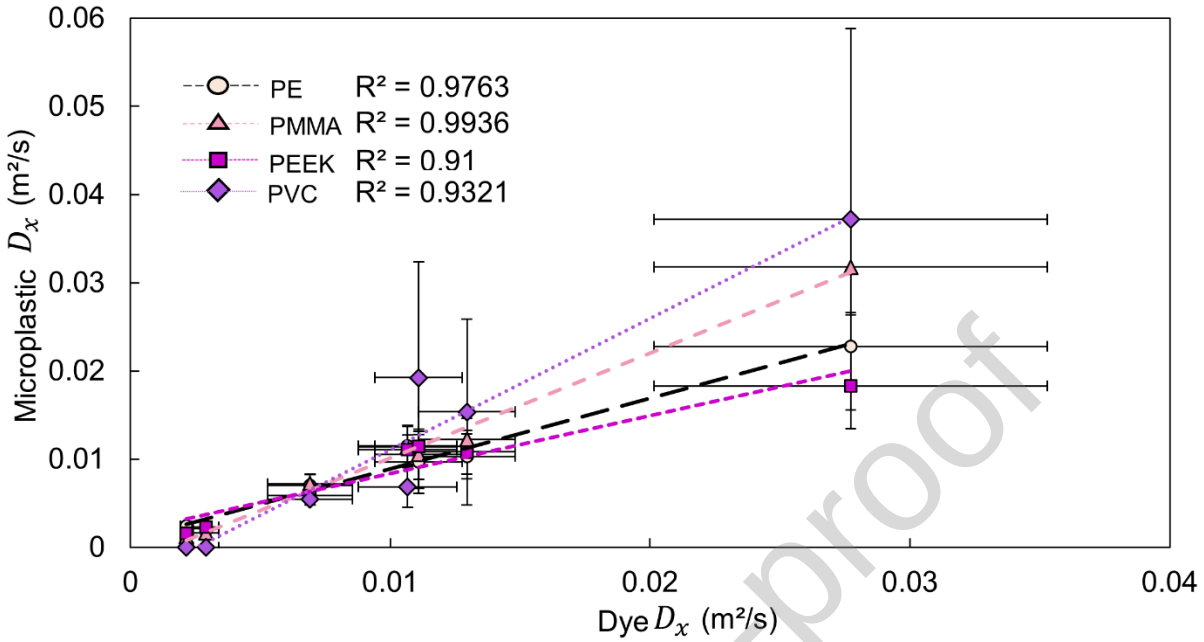

Fig. 9. Mean microplastic longitudinal dispersion coefficients plotted against Rhodamine WT dye (± 95 % confidence intervals)

Declaration of interests

☒ The authors declare that they have no known competing financial interests or personal relationships that could have appeared to influence the work reported in this paper.

☐ The authors declare the following financial interests/personal relationships which may be considered as potential competing interests:

Environmental Implications

Microplastics are emerging contaminants that are ubiquitous to aquatic systems. Given their size, microplastics have increased bioavailability and all aquatic organisms can be exposed through direct ingestion, indirect ingestion via prey items, or respiration. Microplastics can act as a pathway for disease-carrying pathogens and many questions remain as to their toxicity. Microplastic transport and fate in fluvial systems is unknown and thereby which organisms experience the most direct exposure. This study aims to reduce the knowledge gap currently associated with how particle properties affect the transport of microplastics in aquatic flows, to ultimately help remediate their impact on the environment.

Graphical abstract

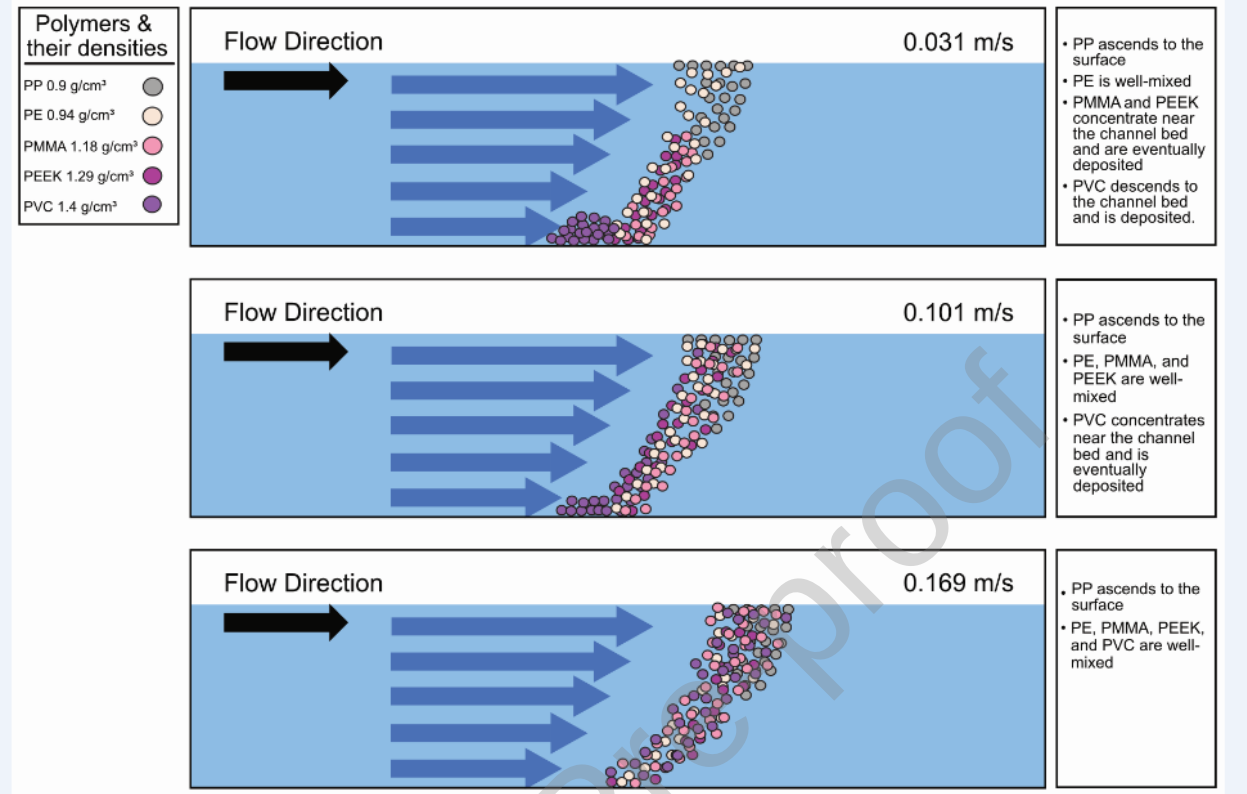

Highlights

- In most conditions, polymers exhibited similar transport characteristics to solutes
- Microplastic deposition was associated with polymer density at velocities ≤ 0.101 m/s
- When deposition occurred, mass recovery was lower near bottom of the water column
- Significant microplastic density thresholds were < 0.94 g/cm³ and > 1.32 g/cm³
- Mixing models and Shields parameters were capable of reliable fate predictions